

# Self-Assembly of Arg–Phe Nanostructures via the Solid–Vapor Phase Method

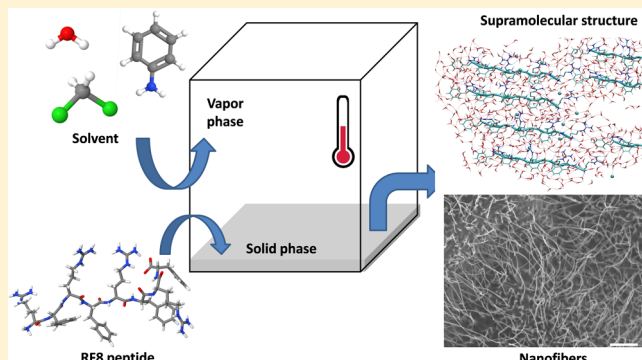
Michelle S. Liberato,<sup>†</sup> Sergio Kogikoski, Jr.,<sup>†</sup> Emerson R. Silva,<sup>†</sup> Mauricio D. Coutinho-Neto,<sup>†</sup> Luis P. B. Scott,<sup>†</sup> Ricardo H. Silva,<sup>†</sup> Vani X. Oliveira, Jr.,<sup>†</sup> Rômulo A. Ando,<sup>‡</sup> and Wendel A. Alves\*,<sup>†</sup>

<sup>†</sup>Centro de Ciências Naturais e Humanas, Universidade Federal do ABC, 09210-170 Santo André, SP, Brazil

<sup>‡</sup>Instituto de Química, Universidade de São Paulo, C.P. 26077, 05513-970 São Paulo, SP, Brazil

## Supporting Information

**ABSTRACT:** We report for the first time on the self-assembly of nanostructures composed exclusively of alternating positively charged and hydrophobic amino acids. A novel arginine/phenylalanine octapeptide, RF8, was synthesized. Because the low hydrophobicity of this sequence makes its spontaneous ordering through solution-based methods difficult, a recently proposed solid–vapor approach was used to obtain nanometric architectures on ITO/PET substrates. The formation of the nanostructures was investigated under different preparation conditions, specifically, under different gas-phase solvents (aniline, water, and dichloromethane), different peptide concentrations in the precursor solution, and different incubation times. The stability of the assemblies was experimentally studied by electron microscopy and thermogravimetric analysis coupled with mass spectrometry. The secondary structure was assessed by infrared and Raman spectroscopy, and the arrays were found to assume an antiparallel  $\beta$ -sheet conformation. FEG-SEM images clearly reveal the appearance of fibrillar structures that form extensive homogeneously distributed networks. A close relationship between the morphology and preparation parameters was found, and a concentration-triggered mechanism was suggested. Molecular dynamics simulations were performed to address the thermal stability and nature of intermolecular interactions of the putative assembly structure. Results obtained when water is considered as solvent shows that a stable lamellar structure is formed containing a thin layer of water in between the RF8 peptides that is stabilized by H-bonding.



## INTRODUCTION

Peptides are perhaps the most versatile building blocks for the self-assembly of bioinspired nanostructures due to their chemical diversity and inherent ability to effectively interface with biological systems.<sup>1</sup> Numerous reports are available on the use of cyclic, amphiphilic, bolaamphiphilic, ionic, surfactant-like, and hydrophobic peptides for the production of nanostructures.<sup>2–7</sup> In addition, the conjugation of these arrays with transition metals, polymers, and photoluminescent compounds, among others, substantially increases their range of applications.<sup>8–10</sup>

Among several strategies for the self-assembly of peptides, the solid–vapor method recently proposed by Ryu et al.<sup>11</sup> is an interesting one. This approach comprises two steps: in the first step, an amorphous film is formed on the surface of a solid substrate through the simple deposition of a volatile solution that contains the peptide building blocks. The self-assembly occurs during the second step, when the samples are incubated under an atmosphere saturated with the vapor of a second solvent. In this stage, molecules from the gas phase act as mediators for intermolecular interactions between peptide units and, associated with the limited mass transport in the solid phase, lead to the slow growth of self-ordered structures around

surface-confined nucleation centers.<sup>12</sup> Interestingly, the lack of strong hydrophobic forces, which are typically predominant in liquid-phase methods, opens an experimental window to probe the role of other intermolecular interactions in the self-assembly.

Phenylalanine (F) is the most commonly used  $\alpha$ -amino acid for the building of peptidic structures. This aromatic molecule is the basic unit of the L-diphenylalanine enantiomer, which is a short dipeptide found in the core recognition motif of the Alzheimer's  $\beta$ -amyloid fibrils.<sup>13</sup> It can self-assemble into a large variety of ordered architectures,<sup>14</sup> among which, one-dimensional symmetries (nanotubes, nanowires, and nanoribbons) are the most commonly found. The structures are maintained by inter- and intramolecular forces, such as H-bonds, Coulomb, and  $\pi$ -stacking interactions.

Peptide sequences that contain arginine (R) have attracted interest during the past decade because of their high potential as cargo-transporters for intracellular delivery.<sup>15</sup> Both proteic and nucleic acid segments, DNA and RNA, have been successfully

Received: August 3, 2012

Revised: December 21, 2012

Published: January 3, 2013

transfected by conjugation with R-containing peptides.<sup>16</sup> In addition to these potentialities, arginine exhibits other features that make it interesting for the study reported here. The abundance of NH-containing groups makes its side chain highly versatile for the intermolecular synergism. Specifically, these groups behave in a distinguished manner with respect to their interactions with aromatic rings. The guanidinium units have appreciable capability to donate H-bonds. H-bonds between amino and aromatic groups have been demonstrated to be relevant in a wide range of biological structures, particularly in protein interfaces, where the amino groups tend to be positioned near benzenic units.<sup>17</sup> When the NH-containing groups are positively charged, the interplay between them and aromatic rings is especially favored and strong cation- $\pi$  interactions can arise.<sup>18</sup>

In the current work, we take advantage of both the ability of guanidinium to donate H-bonds and the propensity of aromatic rings for establishing  $\pi$ -stack interactions to build nanometric structures from mixed Arg/Phe sequences. We report on the synthesis of a linear peptidic sequence obtained through the intercalation of R and F amino acids to form an octapeptide, RF8 (abbreviated Ac-RFRRFRF). We use these building blocks to attain self-ordered nanostructures. Interestingly, the self-assembly reported here contradicts the previous literature that states that peptides composed exclusively of alternating positively charged and hydrophobic residues only form disordered precipitates and not organized structures.<sup>19</sup> Because the combination of R and F residues leads to a hybrid sequence that possesses both hydrophilic and hydrophobic branches, liquid-phase approaches that rely on hydrophobic effects to drive the self-assembly are not appropriate for obtaining ordered structures. To circumvent this drawback, we used the solid-vapor phase strategy. We present a detailed characterization of the resulting structures. Our data show that RF8 clearly self-associates on the solid substrates in the presence of aniline, water, and dichloromethane vapors. The stability of the structures is experimentally studied by electron microscopy and thermogravimetric analysis coupled with mass spectrometry to evaluate the composition of the evolved gases. The vibrational spectroscopic behavior is also investigated to identify and determine structural variations. Molecular dynamics (MD) simulations were performed to tentatively address the formation and thermal stability of a putative lamellar structure from a theoretical perspective.

## EXPERIMENTAL METHODS

**Materials.** All reagents and solvents were of analytical grade and were used as received. 1,1,1,3,3-Hexafluoro-2-propanol (HFP) was purchased from Fluka. The peptides were synthesized using chloromethyl resin (Merrifield), which was purchased from Advanced Chemtech; the substitution degree of the resin was 0.90 mmol/g, and the peptide was already coupled to the starting amino acid. The protected amino acids used in this study were [(Boc-Phe-OH)] and [(Boc-Arg(Tos)-OH)], both purchased from Sigma-Aldrich.

**Synthesis of the RF8 Compound.** The peptide sequence was synthesized through the *t*-Boc strategy in the solid phase, as proposed by Merrifield.<sup>20</sup> The  $\text{N}\alpha$ -terminal was removed by reaction with 50% trifluoroacetic acid (TFA) in dichloromethane (DCM) in the presence of 2% anisole for 20 min. Couplings were performed with a 2.5-fold excess of 1,3-diisopropylcarbodiimide/*N*-hydroxybenzotriazole (DIC/HOBt) in DCM-dimethylformamide (DMF) (1:1, v/v); the

coupling reactions were monitored with the Kaiser ninhydrin test. To keep the peptidyl resin positive, it was subjected to acetylation with 25% acetic anhydride in DMF with excess DIEA (diisopropylethylamine) for 20 min. Dry-protected peptidyl resin was exposed to 70% TFA + 20% TFMSA (4-trifluoromethane sulfonic acid) + 10% anisole for 12 h at 4 °C. Crude lyophilized peptide was then purified by reverse-phase HPLC in aqueous solutions of ACN/0.1% TFA (60:40) on a Waters Delta Prep 600 system, having purity above 96%. Purified peptides were characterized by liquid-chromatography electrospray-ionization mass spectrometry, LC/ESI-MS: RF8 [MM + H] = 1274 (calcd = 1273.5) (see Supporting Information).

**Nanostructuration Process.** The nanostructures were prepared through an adapted form of the solid-vapor method recently proposed by Ryu and Park<sup>11,21</sup> and described elsewhere.<sup>22</sup> Precursor solutions were obtained by dissolving the RF8 monomers in HFP at concentrations of 50, 100, and 150 mg mL<sup>-1</sup>. To avoid aggregation, fresh mixtures were prepared before each experiment. Droplets from the solutions were deposited on ITO substrates modified with PET and dried overnight at room temperature in a vacuum desiccator. This step led to the formation of amorphous peptidic films on the ITO/PET surfaces. In a subsequent stage, the substrates were incubated under an atmosphere saturated with the vapor of a second solvent: aniline, water, or DCM. The wafers with the films were carefully placed in sample holders suspended within glass beakers that contained ~10 mL of the appropriate solvent. The beakers were covered with aluminum foil, and only the vapor, not the liquid, reached the film. The sets were incubated under normal pressure in a muffle furnace whose temperature was maintained at 98 °C when aniline or water vapor was used or at 35 °C when DCM was the solvent in the gas phase.

**Electron Microscopy.** Scanning electron microscopy (SEM) images were collected using an FEG-SEM (JSM 6330F) microscope at the LME/LNLS (Laboratory of Electron Microscopy at the Brazilian synchrotron facility in Campinas, Brazil). The acceleration voltage was 5 kV, and the samples were previously coated with Au layers.

**Spectroscopic Techniques.** Fourier-transform infrared (FT-IR) spectra were obtained on a Varian 660 FTIR spectrophotometer located at the experimental multiuser platform of UFABC. The ATR-FTIR spectra were collected by pressing the powder sample into contact with ZnSe element. All spectra were obtained at 50 scans and with a resolution of 2 cm<sup>-1</sup> in the range between 650 and 1800 cm<sup>-1</sup>. Raman spectroscopy was performed on a Renishaw inVia Raman equipped with a CCD detector and coupled to a Leica microscope (BTH2) at the experimental multiuser platform of IQ/USP. The excitation wavelength was 785 nm and was provided by a Renishaw model HPNIR785 laser. The laser beam was focused on the sample by a 100 $\times$  objective. The power was maintained at 15  $\mu\text{W}$  to avoid sample degradation, and 20 scans of 10 s each of integration time were used. The analysis of the Raman spectra, as well as the baseline correction, was performed using the Grams7.0 software.

**Computational Simulation Procedure.** Explicit solvent MD simulations were performed to investigate the stability of a tentative structure for the peptide assembly in water. All MD investigations were performed using the SPC water model and the GROMOS 96.53a6 classical force field.<sup>23,24</sup> The peptides were protonated under a pH = 2 to match the experimental conditions. The procedure to build an initial peptide strand was

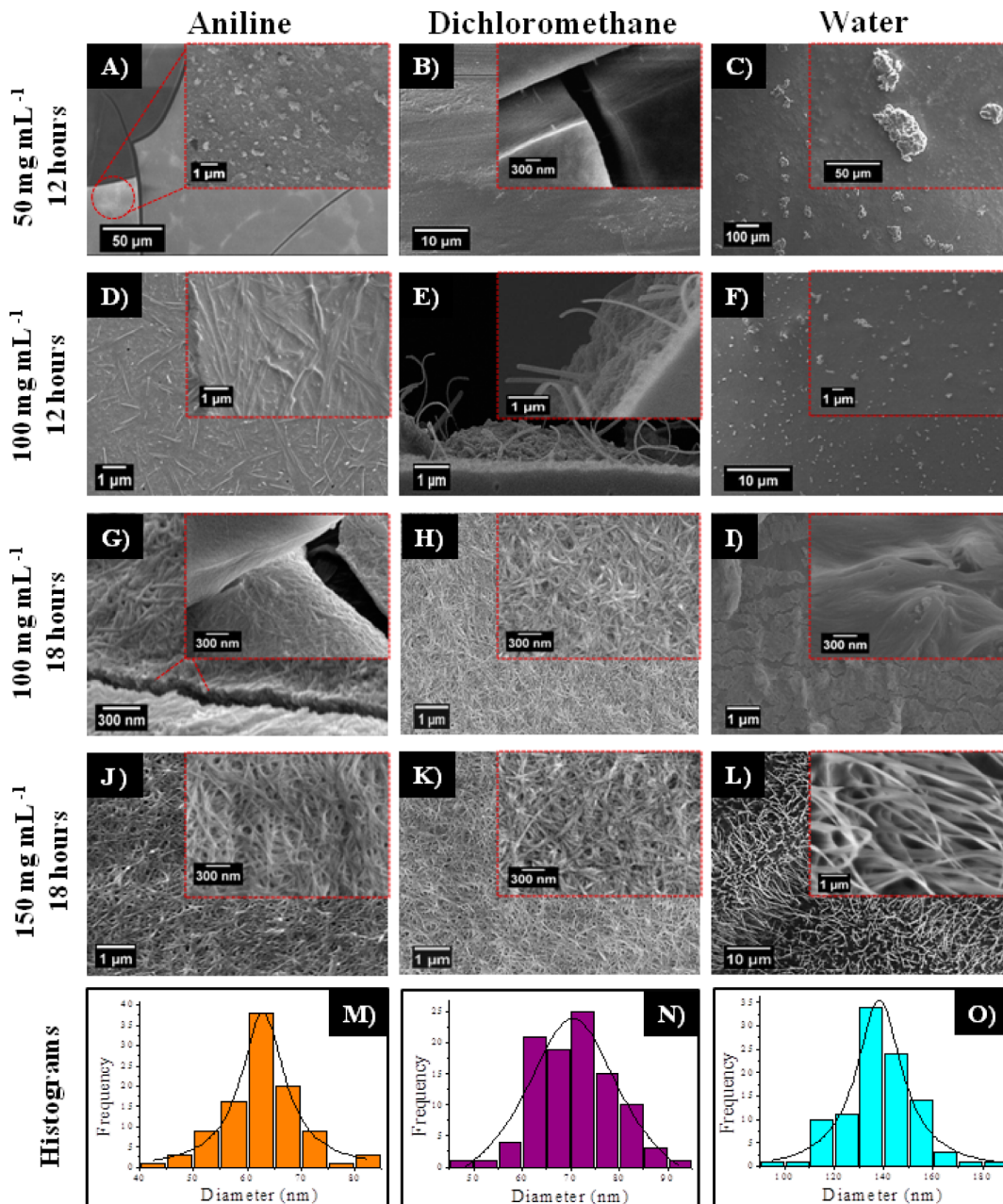


**Figure 1.** (A–L) FEG-SEM images showing the morphology of structures grown on ITO/PET substrates. The experimental conditions are stated on the sides of the figure. In the bottom row, histograms with the distributions of the diameters for the structures grown at a concentration of 150 mg mL<sup>-1</sup> and incubated for 18 h under (M) aniline, (N) dichloromethane, and (O) water vapor are shown.

divided into two stages:<sup>25</sup> (i) minimization with the method of steepest descent, (ii) minimization by the conjugate gradient method, and (iii) a short MD of 1 ns in explicit solvent. The proposed initial configuration was motivated by the evidence that the assemblies form fibrillar structures and show an enhanced IR signal from guanidinium groups being partially aligned. The structure was built with 10 individual strands obtained from the minimization/MD described above, being 8 copies in a side-by-side configuration and 2 copies on a top-bottom configuration (see Figure 3). The distance between strands was initially set to ~8 Å. MD was followed at three distinct temperatures, namely, 98, 120, and 150 °C. Chloride counterions were added to neutralize the system. Motivated by previous evidence that a thin layer of liquid water is present at the solid–vapor interface where the self-assembly occurs,<sup>26</sup> MD

simulations were performed in liquid water. To simulate the liquid state at temperatures above the boiling point of the solvent, the pressure was increased in the MD simulations carried out at 120 and 150 °C to, respectively, 2 and 5 atm. At 98 °C, the standard value of 1 atm was used.

**Thermal Analyses.** Mass-coupled thermogravimetric analyses (TG-MS) were recorded on a Netzsch thermoanalyzer, model TGA/DSC 490 PC Luxx, coupled to an Aëlos 403C mass spectrometer at the Institute of Chemistry, Universidade de São Paulo (IQ-USP), using a heating rate of 10 °C/min and a synthetic air flow of 50 mL/min.

## RESULTS AND DISCUSSION

**Morphological Characterization.** As previously discussed, the RF8 monomer is a hybrid sequence composed of

both hydrophilic and hydrophobic residues. This duality becomes the self-assembly through liquid-phase methods with difficulty because it does not allow for strong hydrophobic effects to drive the peptide ordering.<sup>27</sup> Following the scale developed by Tao et al.,<sup>28</sup> where the overall hydrophobicity is obtained by summing the contributions of the component amino acids, the sequence reported here has a hydrophobicity of  $\sim 0.3$ . For comparison, according to this same scale, the hydrophobicity of FF dipeptides, which are widely used for building nanostructures through liquid-phase approaches, is  $\sim 1.13$ . We failed in several attempts to obtain self-ordered structures through solution-based methods, even after using a wide range of peptide concentrations in both polar and nonpolar solvents, e.g., water, ethanol, methanol, propanol, butanol, acetic acid, chloroform, acetonitrile, DMSO, toluene, and DMF. We hypothesize that the lower hydrophobicity of the RF8 monomer, combined with the presence of positive charges, caused this sequence to be easily solvated and prevented spontaneous ordering in the liquid phase. To address this problem, we used the solid–vapor method proposed by Ryu et al.,<sup>11</sup> which is described in the Experimental Methods section. Notably, with this strategy, the self-assembly appears to be mediated by the solvent in the gaseous phase, which could improve the role of other noncovalent bonds instead of hydrophobic interactions (e.g., H-bonds, dipole–dipole and van der Waals forces,  $\pi$ -stacking, and so on).<sup>11</sup>

In Figure 1, we present electron microscopy images from samples after they were subjected to the solid–vapor approach. The parameters used in the preparation, specifically, the peptide concentration in the precursor solution, the incubation time, and the solvent in the vapor phase are also displayed on the sides of the figure. We begin by discussing the self-assembly in films incubated for 12 h and prepared from solutions with a concentration of  $50 \text{ mg mL}^{-1}$ ; Figure 1A–C. Despite of the appearance of tiny clusters when water vapor was used, the formation of self-ordered architectures is not observed. We attribute this absence of regular structures to the low concentration of peptides, which would not be sufficient to trigger a super saturation-driven growth at the surface.<sup>29</sup> As mentioned in the Introduction, the growth of nanostructures requires nucleation centers on the surface of the amorphous film. Thus, the low concentration of peptide undermines the formation of the seeds around which the self-assembly would occur. We subsequently investigated films prepared from solutions with a concentration of  $100 \text{ mg mL}^{-1}$ ; Figure 1D–F. Unlike the low-concentration case, a discrete nucleation of nanosized structures is observed for samples subjected to DCM and aniline vapors. However, for samples subjected to water-vapor incubation, the formation of nanostructures is not observed. These observations provide clear evidence of the presence of a super saturation-driven mechanism for the self-assembly reported here. Amino acids are more soluble in water than in the other organic solvents used in the gas phase. Thus, the super saturation required to form nucleation centers is reached earlier when DCM or aniline is used as the vapor-phase solvent.

As a further step, we increased the incubation time to 18 h. Because self-assembly was not previously observed in films prepared from  $50 \text{ mg mL}^{-1}$  solutions, this concentration was not evaluated in this second stage. Figures 1G–I present the resulting morphologies of films obtained from solutions that contained RF8 at  $100 \text{ mg mL}^{-1}$ . A comparison between these images and those obtained after 12 h reveals an increase in the

number of structures per area in the samples exposed to organic vapors (cf. Figure 1D,G,E,H). In addition, the coating appears to be homogeneously distributed across the substrate with the formation of an intricate network of fibrillar structures. In the sample exposed to water vapor, some changes in the morphology of the film are evident, such as the disappearance of the previously observed clusters. Nevertheless, we did not observe noticeable nanostructures; Figure 1I.

We also studied the behavior of films prepared from RF8 solutions at  $150 \text{ mg mL}^{-1}$ . The corresponding FEG-SEM images are presented in Figure 1J–L. The formation of dense networks that cover the substrates is again observed in samples kept under organic vapors in a manner similar to that previously observed. The difference in these trials with a higher peptidic concentration is related to the sample incubated under water steam. Unlike the previous results, the clear formation of one-dimensional structures on the surface is now observed, as in Figure 1L, which confirms that a concentration dependence triggers the self-assembly.

In all of the previously described cases, the predominant morphology corresponds to fibrillar structures. Statistical analysis of the sizes of the assemblies reveals that the average thicknesses are  $62.3 \pm 7.2$  and  $71.0 \pm 8.0 \text{ nm}$  for structures grown under aniline and DCM, respectively. When water vapor is used, the dimensions of the arrays increase significantly and reach a highly monodisperse average thickness of  $139.5 \pm 1.5 \text{ nm}$ . To tentatively explain this increase in the dimensions of the structures, we present two conjectures: First, the effect could be related to a shield-like effect. Because DCM and aniline have a lower dipole moment in comparison to that of water ( $1.6$  and  $1.53$  vs  $1.85 \text{ D}$ ) in the gas phase, respectively,<sup>30</sup> they are less efficient in mediating dipole–dipole interactions between peptide molecules. Thus, the positive charges in the Arg side chains are less visible to the other charged groups and screen the intensity of these forces. Second, the effect could be related to the dielectric constant ( $\epsilon$ ) of each solvent. DCM and aniline have comparable values for  $\epsilon$ :  $\sim 8.4$  (at  $35^\circ\text{C}$ ) and  $\sim 5.5$  (at  $98^\circ\text{C}$ ), respectively.<sup>31</sup> In contrast, water has a significantly higher dielectric constant,  $\epsilon \approx 55$  (at  $98^\circ\text{C}$ ).<sup>32</sup> In this case, Coulombic repulsion would be significantly lower when the interactions between peptide building blocks are mediated by  $\text{H}_2\text{O}$  molecules. Moreover, the presence of water intercalated into the matrix of the assemblies would stimulate the formation of H-bonds, which would account for the self-assembly of larger structures.<sup>33</sup> This close relationship between the morphology and dielectric constant has also been observed for nano-assemblies formed via liquid-phase approaches.<sup>27,34</sup>

Another interesting feature of the fibrils obtained here concerns their flexibility properties. Unlike nanostructures built exclusively from nonpolar building blocks,<sup>11,35</sup> which are typically endowed with high mechanical strengths, our assemblies appear to be highly flexible. This statement is supported by the observation of sinuousness along the fibers, which leads to low persistence lengths. Therefore, the introduction of arginine into the peptide sequence appears to significantly change the elastic properties of the resulting assemblies. This behavior may be related to the presence of cavities in the peptidic matrix at the supramolecular level, as discussed below in the section that details the molecular dynamics trials.

**FT-IR and Raman Spectroscopy.** The secondary structure of the RF8 compound in amorphous and nanostructured films was also studied using FT-IR spectroscopy. IR spectroscopy

provides information about the polar groups of the peptide, the side chain of the arginine, and, especially, the linkage of the amide groups between residues. FT-IR spectra from amorphous and nanostructured films are shown in Figure 2A. The spectral

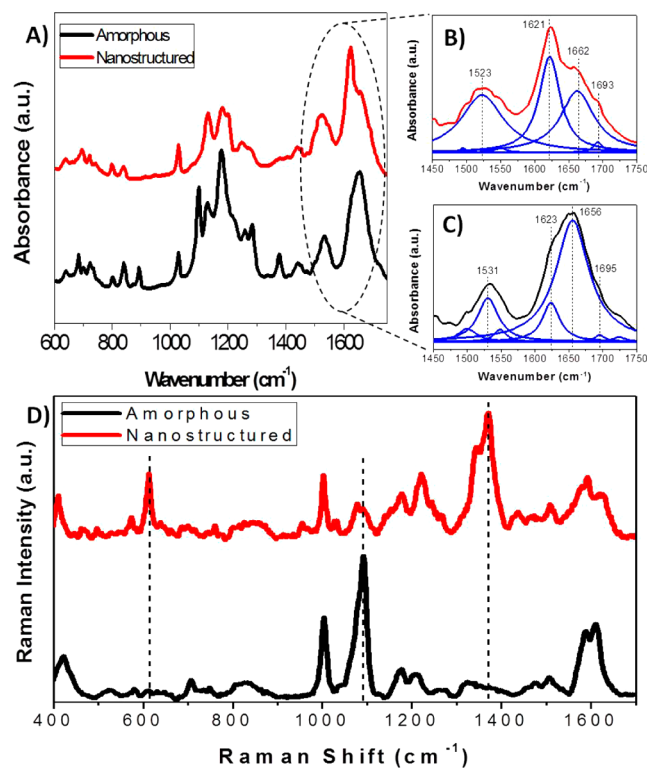


**Figure 2.** FT-IR spectra for amorphous and nanostructured peptides (A). Details for the amine I and II bands are shown (B) for nonstructured and (C) for self-assembled RF8. Blue lines correspond to Lorentzian deconvolution. (D) Raman spectra of both amorphous and self-ordered peptides.

differences are concentrated in the amide I, II, and III regions. Nevertheless, because of the complexity of the IR spectra between 1200 and 1400 cm<sup>-1</sup> (vibrations in this region are often coupled to other modes), this region was not included in this study. The amide I and II domains of the RF8 peptide nanofibers are shown in Figure 2B,C, together with the deconvolution Lorentzian profiles obtained through an interactive curve-fitting procedure.<sup>36</sup> The amide I band, from 1600 to 1700 cm<sup>-1</sup>, shows the contribution of the C=O bond to the secondary structure. We observe a prominent band at 1622 cm<sup>-1</sup> accompanied with a shoulder at 1695 cm<sup>-1</sup> in the amorphous peptide spectrum. These bands correspond to the typical signature of the antiparallel  $\beta$ -sheet conformation.<sup>37</sup> The vibrations of guanidinium groups in the side chain of Arg residues appear at 1656 cm<sup>-1</sup>. Similarly, the amide II band in the 1500–1600 cm<sup>-1</sup> region also suggests the antiparallel  $\beta$ -sheet structure, as demonstrated by an N–H resonance at 1531 cm<sup>-1</sup> (Figure 2C).<sup>36,38</sup>

After the self-assembly, numerous changes are observed in both regions. In the amide I band, modifications are noticed in the relative intensities of the bands. This finding is likely due to the in-phase coupled mode of molecular C=O vibrations leading to an increase in the intensity. Similarly, the intensity of the amide II band is also enhanced.<sup>37a</sup> Shifts are also observed in these bands: in the amide I band, the vibration of the guanidinium ions shifts by 6 cm<sup>-1</sup> to 1662 cm<sup>-1</sup>, and in the amide II band, the N–H vibration shifts by 8 cm<sup>-1</sup> to 1523 cm<sup>-1</sup>. These displacements are probably due to the strengthening of intermolecular interactions between these groups with solvent molecules. Moreover, they may be related to changes in the configuration of the RF8 monomers, as revealed in the subsequent MD simulations, Figure 3A,B, where the self-assembly leads to a high constriction of the molecules. These results corroborate the SEM results and the previously published FT-IR analyses.<sup>36,39</sup>

Raman spectra from these dry films are also shown in Figure 2D. This technique was used because it accounts for the

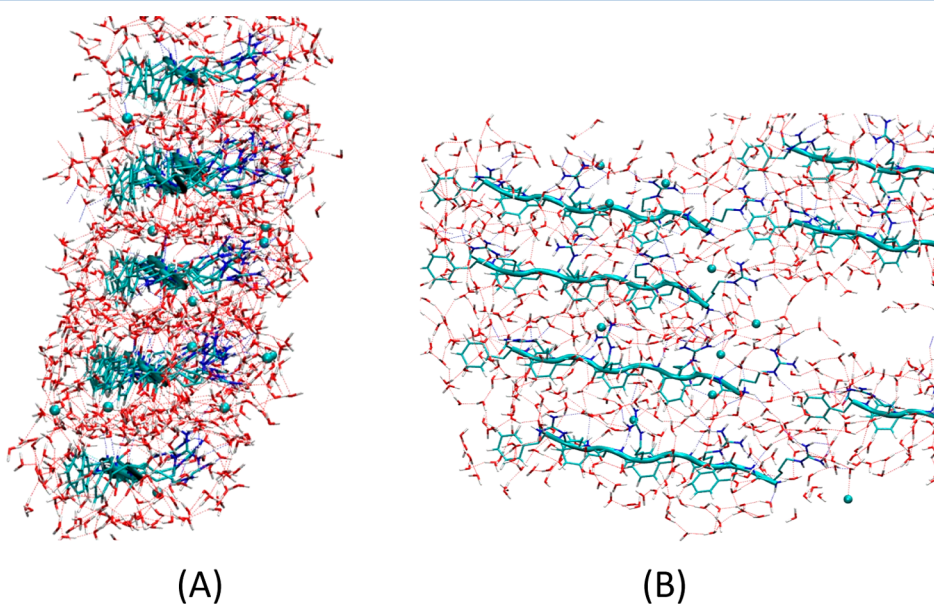


**Figure 3.** Representative frame from MD run at 120 °C showing the H-Bond network between the peptide strands and the nearby water (closer than 4 Å). (A) Side view and (B) top view from the same frame. The peptide is depicted using bonds and cartoon representation, while the water is represented using bonds. H-Bonds are represented as dotted lines connecting the atoms involved.

vibrations of groups with low polarity, such as the phenyl rings of Phe, and it solves the problem of the vibrations of the guanidinium ions being coupled with the amide bands. One of the main differences with respect to the IR data arises from a polarization process that occurs on the side chains. The band at approximately  $600\text{ cm}^{-1}$  is more intense because of the coupled vibration tensor of the phenyl rings.<sup>39</sup> As shown in Figure 3A, the aromatic rings have a preferential orientation after the self-assembly process. A similar process occurs with the bands at  $1091$  and  $1370\text{ cm}^{-1}$ . These bands are characteristic of guanidinium ions and the aliphatic chains of R residues, respectively. The peak at  $1091\text{ cm}^{-1}$  decreases in intensity presumably because of the positions that the guanidinium ions assume after the self-assembly. For the band at  $1370\text{ cm}^{-1}$ , the same situation occurs, but in the opposite manner: the assumed positions lead to an increase in the vibration tensor, which typically occurs in materials with a well-defined crystallographic lattice.<sup>39,40</sup>

**Molecular Dynamics Simulations.** MD calculations using the initial setup described in the Experimental Methods section were propagated for 5 ns at temperatures of  $90$  and  $150\text{ }^\circ\text{C}$ , and for 8 ns at  $120\text{ }^\circ\text{C}$ . The small standard deviations of the root-mean-square deviation (rmsd), below 0.03 nm for all runs, point out the convergence of the formed structures. MD results at all temperatures suggest a very stable lamellar assembly with a  $\beta$ -sheet-like conformation. The presence of a thin  $\text{H}_2\text{O}$  layer in between peptide chains is a remarkable feature of the array, as shown in Figure 3. A network of H-bonds involving this aqueous coating presumably is responsible for the structural stability of the system.

We observe only a slight growth in rmsd values upon increasing temperature (see Figure 4). The radius of gyration, Figure 4 middle, behaves in the very same manner, with a small increase of  $\sim 0.5\text{ \AA}$  when temperature is changed from  $98$  to

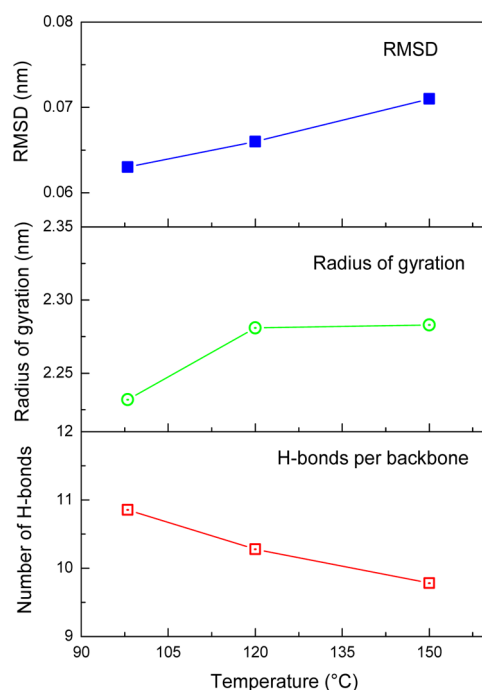


**Figure 4.** Temperature dependence of the average of rmsd (top), radius of gyration (middle), and number of H-bonds per peptide backbone (bottom).

$120\text{ }^\circ\text{C}$ . Nevertheless, the behavior of the number of H-bonds per backbone is quite different with a tendency of reduction at higher temperatures. By one side, the number of direct bonds between strands is negligible at all temperatures. By the other, the number of interactions between N and O atoms in the backbone and  $\text{H}_2\text{O}$  molecules embedded in the peptide matrix appears to be significant. Specifically, the average over the dynamics shows the formation of  $\sim 1/2$  H-bond per NH group (34 H-bonds for 70 groups, at  $98$  and  $120\text{ }^\circ\text{C}$ ) and  $\sim 1$  H-bond per oxygen in the backbone (65 H-bonds for 70 groups at  $120\text{ }^\circ\text{C}$ ). The increase in temperature up to  $150\text{ }^\circ\text{C}$  leads to a diminution of the number of H-bonds for these two groups by a factor of  $\sim 10\%$  when compared to the run at  $120\text{ }^\circ\text{C}$  (see Figure 4, bottom). This finding is consistent with TGA results (following section) that show a loss of water starting at  $120\text{ }^\circ\text{C}$  and maxing out at  $150\text{ }^\circ\text{C}$ .

Negative counterions close to guanidinium groups promote the shield of electrostatic repulsion between cationic charges and gives rise to an additive contribution to the overall stability. Furthermore, guanidinium units in the side-chains of Arg residues also make H-bonds with the interstrand water layer, attesting to the intricate nature of interactions involved in the stabilization of the proposed structure.

**Thermogravimetric and Mass Spectrometry Analyses.** Figure 5A shows the TGA, MS, and DTG data from nanostructures obtained under aniline vapor. We observe two weight losses at  $50$  and  $120\text{ }^\circ\text{C}$ . These mass losses, which are clearly observable in the DTG plot, are ascribed to the release of residual water from the synthesis of RF8 that remained adsorbed and intercalated within the peptidic matrix. This conclusion is supported by MS curves at  $m/z = 18$ , the mass-to-charge ratio of  $\text{H}_2\text{O}$  molecules. The release of water is estimated as  $\sim 0.5\text{ wt \%}$  at  $60\text{ }^\circ\text{C}$  and  $\sim 3.0\text{ wt \%}$  at  $150\text{ }^\circ\text{C}$ . These losses correspond to  $\sim 0.33$  mols of  $\text{H}_2\text{O}$  in the first peak and  $\sim 2$  mols in the second peak. A third appreciable reduction in weight of approximately  $13.5$  to  $41.5\text{ wt \%}$  occurs between  $240$  and  $330\text{ }^\circ\text{C}$  and is attributed to the gradual decomposition of the RF8 nanofibers, which is characterized by water liberation followed by a  $\text{CO}_2$  release step.

To examine the effect of dry heat at  $120\text{ }^\circ\text{C}$  and the influence of water on the morphology of the RF8 nanostructured films, microstructural analyses were performed using FEG-SEM (see Figure 5B). We observed a loss of their structural integrity, even at  $120\text{ }^\circ\text{C}$ , which may be related to the evaporation of water at high temperatures and the consequent disruption of the fibrillar structures. The interactions between peptide side chains are subtle and highly sensitive to hydration, especially when the self-assembly occurs in a nanoscopic confined space. In physically confined environments, confinement effects have been shown to play dominant roles with respect to molecular organization.<sup>41</sup>

## CONCLUSIONS

We have presented evidence for the self-assembly of nanofibers obtained from Arg–Phe building blocks. To the best of our knowledge, this work represents the first time that self-ordered structures have been built from peptides composed exclusively of positively charged and hydrophobic amino acids. A novel octapeptide, RF8, was synthesized. Because the high solubility of this sequence prevents its self-assembly through solution-based approaches, the use of the solid–vapor phase strategy appears to be of underlying importance to attain long, interconnected, nanofibrillar networks on ITO/PET substrates.

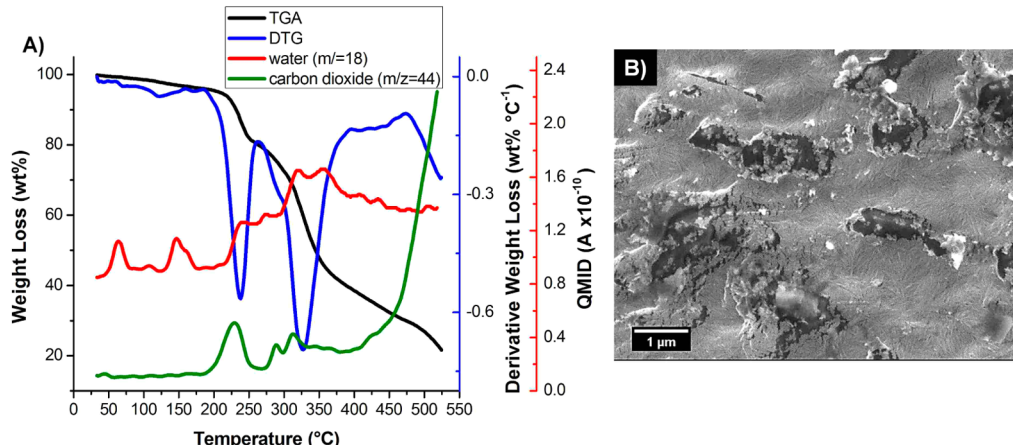


**Figure 5.** (A) TG/DTG curves and mass spectrometry results for nanostructures grown under aniline vapor. (B) SEM/FEG image showing degradation of the structures at 120 °C.

FT-IR and Raman spectroscopy revealed that the monomers are organized according to an antiparallel  $\beta$ -sheet-like conformation.

A close relationship between the morphology of the films and the physicochemical parameters used in their preparation was observed. Specifically, we observed a concentration-based mechanism in which large concentrations of peptides are necessary to trigger the self-assembly. The nature of the solvent in the gas phase was also found to play a paramount role with respect to the morphology. We verified that the use of water vapor leads to the formation of thicker fibrils in structures prepared under aniline or dichloromethane vapors. We speculate that this finding is evidence for H<sub>2</sub>O molecules as strong mediators of H-bonds between peptides. Thermogravimetric and mass spectrometry data corroborate this statement by demonstrating that the release of water destabilizes the nanofibers.

Molecular dynamics simulations provided interesting insights about the organization of RF8 monomers within the assemblies. They suggest that the peptide strands are organized according to a lamellar structure. In addition, these theoretical results corroborate the experimental findings and show that H<sub>2</sub>O molecules embedded in the peptide matrix mediate H-bonds between RF8 backbones and play an important role on the stabilization of the structures. We believe that the special ability of guanidinium groups in donating H-bonds also strongly contributes to the self-assembly reported here.

## ■ ASSOCIATED CONTENT

### Supporting Information

Characterization of the RF8 compound. This material is available free of charge via the Internet at <http://pubs.acs.org>.

## ■ AUTHOR INFORMATION

### Corresponding Author

\*Tel: +55 11 4996 0193. Fax: +55 11 4996 3166. E-mail: wendel.alves@ufabc.edu.br.

### Notes

The authors declare no competing financial interest.

## ■ ACKNOWLEDGMENTS

Financial support by the Brazilian agencies Fundação de Amparo à Pesquisa do Estado de São Paulo (FAPESP, Grants

No. 08/53576-9, 10/09306-7, 09/12153-0, 05/60596-8, and 12/01933-8) is gratefully acknowledged. This work was also supported by INCT Bioanalítica (FAPESP, Grant No. 08/57805-2 and CNPq, Grant No. 573672/2008-3) and CNPq (Grant No. 477806/2010-4). We are thankful to LME-LNLS for the use of SEM facilities.

## ■ REFERENCES

- (1) de la Rica, R.; Matsui, H. *Chem. Soc. Rev.* **2010**, *39*, 3499–3509.
- (2) Toksöz, S.; Guler, M. O. *Nano Today* **2009**, *4*, 458–469.
- (3) Hamley, I. W. *Soft Matter* **2011**, *7*, 4122–4138.
- (4) Kogiso, M.; Okada, Y.; Hanada, T.; Yase, K.; Shimizu, T. *Biochim. Biophys. Acta* **2000**, *1475*, 346–352.
- (5) Papapostolou, D.; Smith, A. M.; Atkins, E. D. T.; Oliver, S. J.; Ryadnov, M. G.; Serpell, L. C.; Woolfson, D. N. *Proc. Natl. Acad. Sci. U.S.A.* **2007**, *104*, 10853–10858.
- (6) Wang, J.; Han, S.; Meng, G.; Xu, H.; Xia, D.; Zhao, X.; Schweins, R.; Lu, J. R. *Soft Matter* **2009**, *5*, 3870–3878.
- (7) Reches, M.; Gazit, E. *Curr. Nanosci.* **2006**, *2*, 105–111.
- (8) Ryu, J.; Park, C. B. *Angew. Chem., Int. Ed.* **2009**, *48*, 4820–4823.
- (9) Ryu, J.; Park, C. B. *Angew. Chem., Int. Ed.* **2009**, *121*, 4914–4917.
- (10) (a) Martins, T. D.; de Souza, M. I.; Cunha, B. B.; Takahashi, P. M.; Ferreira, F. F.; Souza, J. A.; Fileti, E. E.; Alves, W. A. *J. Phys. Chem. C* **2011**, *115*, 7906–7913. (b) Kim, J. H.; Lee, M.; Lee, J. S.; Park, C. B. *Angew. Chem., Int. Ed.* **2012**, *51*, 517–520.
- (11) Ryu, J.; Park, C. B. *Chem. Mater.* **2008**, *20*, 4284–4290.
- (12) Ryu, J.; Park, C. B. *Biotechnol. Bioeng.* **2010**, *105*, 221–230.
- (13) Meital, R.; Ehud, G. *Phys. Biol.* **2006**, *3*, S10–S19.
- (14) (a) Wang, C.; Huang, L.; Wang, L.; Hong, Y.; Sha, Y. *Biopolymers* **2007**, *86*, 23–31. (b) Gokhan, D.; Ugur, T. *Nanotechnology* **2012**, *23*, 225604–225610.
- (15) (a) Hayashi, Y.; Takayama, K.; Suehisa, Y.; Fujita, T.; Nguyen, J.-T.; Futaki, S.; Yamamoto, A.; Kiso, Y. *Bioorg. Med. Chem. Lett.* **2007**, *17*, 5129–5132. (b) Herce, H.; Garcia, A. *J. Biol. Phys.* **2007**, *33*, 345–356.
- (16) (a) Khalil, I. A.; Kogure, K.; Akita, H.; Harashima, H. *Pharmacol. Rev.* **2006**, *58*, 32–45. (b) Hu, J.-W.; Liu, B. R.; Wu, C.-Y.; Lu, S.-W.; Lee, H.-J. *Peptides* **2009**, *30*, 1669–1678.
- (17) (a) Crowley, P. B.; Golovin, A. *Proteins Struct. Funct. Bioinf.* **2005**, *59*, 231–239. (b) Dougherty, D. A. *Science* **1996**, *271*, 163–168. (c) Gallivan, J. P.; Dougherty, D. A. *Proc. Natl. Acad. Sci. U.S.A.* **1999**, *96*, 9459–9464.
- (18) Ma, J. C.; Dougherty, D. A. *Chem. Rev.* **1997**, *97*, 1303–1324.
- (19) (a) Brack, A.; Orgel, L. E. *Nature* **1975**, *256*, 383–387. (b) Bippon, W. B.; Chen, H. H.; Walton, A. G. *J. Mol. Biol.* **1973**, *75*, 369–375. (c) Holmes, T. C.; de Lacalle, S.; Su, X.; Liu, G.; Rich, A.; Zhang, S. *Proc. Natl. Acad. Sci. U.S.A.* **2000**, *97*, 6728–6733.

- (20) Merrifield, R. B. *J. Am. Chem. Soc.* **1964**, *86*, 304–305.  
(21) Ryu, J.; Park, C. B. *Adv. Mater.* **2008**, *20*, 3754–3758.  
(22) Amaral, H. R.; Kogikosky, S., Jr.; Silva, E. R.; Souza, J. A.; Alves, W. A. *Mater. Chem. Phys.* **2012**, *137*, 628–636.  
(23) Berendsen, H. J. C.; van der Spoel, D.; van Drunen, R. *Comput. Phys. Commun.* **1995**, *91*, 43–56.  
(24) Scott, W. R. P.; Hünenberger, P. H.; Tironi, I. G.; Mark, A. E.; Billeter, S. R.; Fennen, J.; Torda, A. E.; Huber, T.; Krüger, P.; van Gunsteren, W. F. *J. Phys. Chem. A* **1999**, *103*, 3596–3607.  
(25) Miyashita, O.; Onuchic, J. N.; Wolynes, P. G. *Proc. Natl. Acad. Sci. U.S.A.* **2003**, *100*, 12570–12575.  
(26) Ye, M.; Zhang, Y.; Li, H.; Xie, M.; Hu, J. *J. Phys. Chem. B* **2010**, *114*, 15759–15765.  
(27) Demirel, G.; Malvadkar, N.; Demirel, M. C. *Langmuir* **2010**, *26*, 1460–1463.  
(28) Tao, P.; Wang, R.; Lai, L. *J. Mol. Model.* **1999**, *5*, 189–195.  
(29) Reches, M.; Gazit, E. *Nat. Nanotechnol.* **2006**, *1*, 195–200.  
(30) (a) Gregory, J. K.; Clary, D. C.; Liu, K.; Brown, M. G.; Saykally, R. J. *Science* **1997**, *275*, 814–817. (b) Lister, D. G.; Tyler, J. K.; Høg, J. H.; Larsen, N. W. *J. Mol. Struct.* **1974**, *23*, 253–264. (c) Dang, L. X. *J. Chem. Phys.* **1999**, *110*, 10113–10122.  
(31) Hunger, J.; Stoppa, A.; Thoman, A.; Walther, M.; Buchner, R. *Chem. Phys. Lett.* **2009**, *471*, 85–91.  
(32) Ellison, W. J. *J. Phys. Chem. Ref. Data* **2007**, *36*, 1–18.  
(33) Kim, J.; Han, T. H.; Kim, Y.-I.; Park, J. S.; Choi, J.; Churchill, D. G.; Kim, S. O.; Ihhee, H. *Adv. Mater.* **2010**, *22*, 583–587.  
(34) Huang, R.; Qi, W.; Su, R.; Zhao, J.; He, Z. *Soft Matter* **2011**, *7*, 6418–6421.  
(35) Li, H.; Zhang, F.; Zhang, Y.; He, J.; Hu, J. *Acta Biochim. Biophys. Sin.* **2007**, *39*, 285–289.  
(36) Pelton, J. T.; McLean, L. R. *Anal. Biochem.* **2000**, *277*, 167–176.  
(37) (a) Barth, A.; Zscherp, C. Q. *Rev. Biophys.* **2002**, *35*, 369–430.  
(b) Kong, J.; Yu, S. *Acta Biochim. Biophys. Sin.* **2007**, *39*, 549–559.  
(38) (a) Zandomeneghi, G.; Krebs, M. R. H.; McCammon, M. G.; Fändrich, M. *Protein Sci.* **2004**, *13*, 3314–3321. (b) Miyazawa, T.; Blout, E. R. *J. Am. Chem. Soc.* **1961**, *83*, 712–719.  
(39) De Gelder, J.; De Gussem, K.; Vandebaele, P.; Moens, L. J. *Raman Spectrosc.* **2007**, *38*, 1133–1147.  
(40) Faria, J. L. B.; Freire, P. T. C.; Gonçalves, R. O.; Melo, F. E. A.; Mendes-Filho, J.; Lima, R. J. C.; Moreno, A. J. D. *Braz. J. Phys.* **2010**, *40*, 288–294.  
(41) Kim, J.; Han, T. H.; Kim, Y.-I.; Park, J. S.; Choi, J.; Churchill, D. G.; Kim, S. O.; Ihhee, H. *Adv. Mater.* **2010**, *22*, 583–587.